

**Simulating many-body physics with quantum nonlinear optics**Zhe Chen,<sup>1,2</sup> Xiao-Ye Xu,<sup>1,2,3,\*</sup> Qin-Qin Wang,<sup>1,2,3</sup> Yong-Jian Han,<sup>1,2,3,†</sup> Chuan-Feng Li<sup>①,1,2,3,‡</sup> and Guang-Can Guo<sup>1,2,3</sup><sup>1</sup>CAS Key Laboratory of Quantum Information, University of Science and Technology of China, Hefei 230026, China<sup>2</sup>CAS Center for Excellence in Quantum Information and Quantum Physics,  
University of Science and Technology of China, Hefei 230026, China<sup>3</sup>Hefei National Laboratory, University of Science and Technology of China, Hefei 230088, China

(Received 15 December 2022; accepted 8 May 2023; published 18 May 2023)

The rapidly growing field of quantum information can benefit greatly from quantum nonlinear optics, which has the potential to generate highly correlated optical states with a sufficiently large interaction strength per photon. Such states play a crucial role in various quantum applications. While the traditional approach to generating correlated optical states involves controlled interactions between individual single photons through nonlinear mediums, a more efficient approach is to use the evolution of multiphotons in the highly nonlinear optical medium. To facilitate this approach, we propose a scheme that traces the time evolution of the photons encoded in Fock space to generate complex correlated states. Our approach mimics the dynamics of many-body systems with adjustable interaction strength, allowing us to simulate state transfer on a spin chain by tuning the interaction. We also investigate the feasibility of our scheme based on current technologies and explore the potential of quantum nonlinear optics in quantum simulation.

DOI: [10.1103/PhysRevA.107.053711](https://doi.org/10.1103/PhysRevA.107.053711)**I. INTRODUCTION**

The photonic system is widely regarded as an ideal platform for quantum computation and quantum simulation [1] thanks to its long coherent time and accurate single-qubit operation. However, implementing a two-qubit gate between photons still poses a significant challenge due to the difficulty of interaction between them. The Knill-Laflamme-Milburn (KLM) scheme [2] suggests that the two-qubit gate can be realized in linear optics through measurements and bosonic statistics. Nevertheless, its intrinsic probabilistic nature and stringent experimental requirements make it hard to scale up in practice [3]. Alternatively, a strongly nonlinear medium can induce a deterministic two-photon gate when its nonlinear interaction rate exceeds the decoherence rate [4,5]. As a result, the universal quantum computation can be realized through the nonlinear optics in the quantum region [5–7]. Fortunately, recent advancements in materials and technologies [8–14] offer promising avenues for reaching the quantum regime of nonlinear optics.

Though a full-fledged universal quantum computer is not yet available, it is possible to simulate complicated systems in the developing quantum machine based on nonlinear optics. In an analog quantum simulation, the primary task is to establish the correspondence between the desired many-body systems Hamiltonian and the effective Hamiltonian in the quantum simulator [15]. While simulators based on solid-state systems, such as ion traps [16,17], ultra-cold atoms [18,19],

and superconductivity systems [20,21], are easy to realize interactions but hard to maintain quantum coherence, optical simulators have long coherent times but are difficult to implement interactions between photons. The special character of the photonic systems makes it significantly challenging to establish the Hamiltonian correspondence between the many-body systems and the simulator [22].

So far, the primary quantum simulations involving multiphotons, in essence, can be viewed as state preparation [23]. Only a few quantum simulations of noninteraction many-body systems have been carried out, using a single-particle Fock state distributed across various bosonic modes under band theory [24–29]. However, it is believed that the multiphoton states obtained from the interferometer network, which has been used to show quantum supremacy [30,31], can provide potential power to simulate many-body physics efficiently. Recently, researchers demonstrated a quantum simulator that exploited multiphoton states using only a single beam splitter [32]. This simulator was able to simulate many-body dynamics, such as the nonlinear Su-Schrieffer-Heeger (SSH) model and the general chiral  $XY$  spin-1/2 chain. However, this simulator's capability was significantly limited by a fatal shortcoming: the interaction strength of the simulated system cannot be adjusted.

Here we propose a quantum simulation scheme based on multiphoton states obtained in quantum nonlinear optics. This scheme can be used to simulate many-body physics with adjustable interaction strength. By mapping the nonlinear photonic interaction to a spin chain Hamiltonian, we show that the full quantum treatment of quantum nonlinear optics can reveal its connection to many-body physics. The analogy between nonlinear optics and spin-1/2 systems is often used when studying geometric phases in nonlinear optics [33].

\*xuxiaoye@ustc.edu.cn

†smhan@ustc.edu.cn

‡cfli@ustc.edu.cn

However, instead of treating the two modes of light as components of a single spin-1/2, as is typically done, our mapping maps the Hilbert space as the single excitation subspace of a spin-1/2 chain. By taking advantage of this mapping, we establish a preliminary simulation of  $XY$  spin chain dynamics with adjustable coupling.

The rest text is organized as follows. Section II provides a full quantum treatment of a nonlinear process whose Hamiltonian is mapped to a many-body physical system in Sec. III. We then numerically solve this Hamiltonian in Sec. IV to better understand the dynamic behavior of the simulator. As an example, in Sec. V, we examine the state transfer property of the simulated system. Finally, we discuss the practicality of our scheme in terms of experimental implementation.

## II. QUANTIZED HAMILTONIAN IN THE SECOND-ORDER NONLINEAR OPTICAL PROCESSES

Due to the linearity of the electromagnetic field, any light (photon) cannot interact directly and their interaction can only be induced by medium: two lights interact with the medium together to induce the interaction between the two lights. Therefore, the interaction between two lights is the second- or higher-order effect of the interaction between the light and the medium. The higher the order, the weaker the effect. It was previously believed that the third-order ( $\chi^{(3)}$ ) nonlinearity was the minimum required order for implementing optical quantum computation [5]. However, subsequent work has shown that the second-order ( $\chi^{(2)}$ ) nonlinearity is sufficient to accomplish the same task if we take the depleted pump regime into account [6].

A typical scenario of the depleted pump regime is the cascaded down-conversion developed for generating photon triplets without postselection [34]. In this application, the pump field appearing in the second stage parametric down-conversion (PDC) can be treated quantum mechanically because the pump originating from the first stage is so weak that it only has a power of a few hundred femtowatts. In fact, while the weak pump field only contains  $10^6$  photons per second and can be approximated as a single photon state, it is exactly a portion of the two-mode squeezed state generated in the first stage PDC. That is to say, when the second stage PDC is arranged to work at a high squeezing level, the single photon state from the first stage PDC, acts as the pump in second stage PDC, will be used up quickly, and the parametric approximation is no longer applicable.

The depleted pump regime requires low pump power and high nonlinear strength at the same time. However, conventional nonlinear optics adopts bulk crystals whose nonlinear coefficients are extremely small and only show nonlinear effects under a high-energy field. New materials with high nonlinear coefficients and advancements in controlling light fields enable the single-photon-level nonlinearity [9–14], bringing the field into the quantum region [8]. Consequently, the nonlinear optics with depleted pump can be implemented.

We begin with a simple model of a nonlinear medium mediating the second-order nonlinear process shown in Fig. 1(a), which can be described by the Hamiltonian [35]

$$H = \omega_p a_p^\dagger a_p + \omega_i a_i^\dagger a_i + \omega_s a_s^\dagger a_s$$

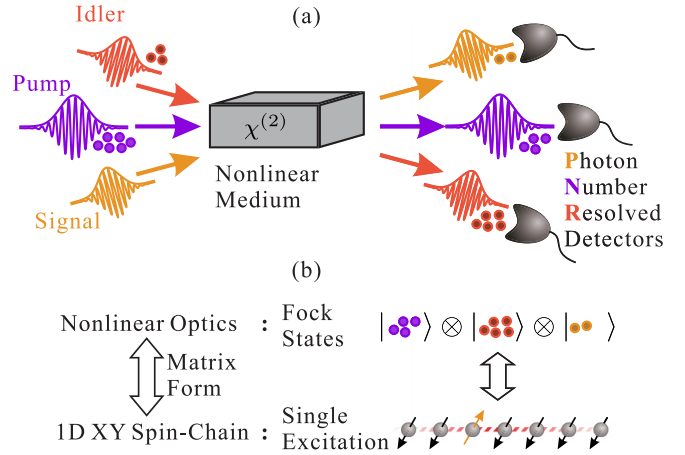


FIG. 1. Nonlinear photonic quantum simulator with Fock states. (a) A nonlinear process mixing three optical modes with Fock-state inputs, following a photon-number-resolved (PNR) detection for readout. (b) Fock states  $|N-n, M+n, n\rangle$  encode a  $N+1$  sites spin- $\frac{1}{2}$  chain with the  $(n+1)$ th spin excited.  $M$  controls the adjustable coupling strength.

$$+ \kappa (a_p a_s^\dagger a_i^\dagger + a_p^\dagger a_s a_i), \quad (1)$$

where we chose units so that  $\hbar = 1$ ;  $a_j^\dagger$  and  $a_j$  denote the creation and annihilation operators acting on the pump, signal, and idler mode in the nonlinear process ( $j = p, s, i$ ), with the corresponding frequencies  $\omega_j$ , and  $\kappa$ , which is assumed to be real valued without loss of generality, stands for the coupling coefficient depending upon the second-order susceptibility tensor  $\chi^{(2)}$ , the geometrical factors of the crystal, and the mode volumes of the involved modes. We can further simplify the Hamiltonian in the interaction picture

$$H_I = \kappa (a_p a_s^\dagger a_i^\dagger + a_p^\dagger a_s a_i), \quad (2)$$

by regarding the linear term  $H_L = \omega_p a_p^\dagger a_p + \omega_i a_i^\dagger a_i + \omega_s a_s^\dagger a_s$  as the free part and using the energy conservation constraint  $\omega_p = \omega_i + \omega_s$ .

When we simplify our analysis, we are neglecting degrees of freedom within each mode. However, when we take these factors into consideration, the energy exchange among all of the modes becomes very complex and solving the dynamics becomes extremely difficult. Despite this, our simplified approach still has practical value. For instance, cavities are generally adopted to enhance the interaction in nonlinear optical processes [36]. The quality factor of these cavities is usually very large, indicating a narrow linewidth. This means that we can treat the two parametric fields as reduced single modes, simplifying the analysis and making it more manageable. The effective mode numbers appearing in an experiment can be estimated in terms of the second-order autocorrelation function  $g^{(2)}(0) = (\langle n^2 \rangle - \langle n \rangle^2) / \langle n \rangle^2$  [37] of the signal under a strong pump, which can be measured experimentally. The single-mode-ness can then be quantified via the effective mode number  $K = 1 / [g^{(2)}(0) - 1]$  [38,39]. For fields obeying thermal statistics,  $g^{(2)}(0) = 2$  indicates an ideal single-mode number  $K = 1$ , while for fields obeying Poissonian statistics,  $g^{(2)}(0) = 1$  gives an infinite mode number. Moving a step further, faithfully following the Hamiltonian Eq. (2) and

treating the pump field quantum mechanically, the relevant time-evolution operator can be directly given as

$$U = e^{-it\kappa(a_p a_s^\dagger a_i^\dagger + a_p^\dagger a_s a_i)}. \quad (3)$$

Different from the squeezing operator obtained under familiar treatment, the time evolution under full quantum treatment transfers the energy among the various bosonic modes. Then we need to consider the exact solution of the time evolution operator rather than standing on an approximation result. Due to the statistics of bosons [40] and the effect involved in calculating the creation and annihilation operators [41,42], exactly calculating the complex amplitude of such quantum scattering of bosons is usually not easy. While some results attempting the full quantum treatment of quantum nonlinear optics were presented for special scenarios [43,44], there is still a lack of general theoretical framework. Here, rather than trying to address the challenges directly, we restrict the form of optical modes and input states in the nonlinear process.

To simplify the analysis, we consider that the pump pulse contains a definite photon number  $n_p$ , which corresponds to an infinite number-phase squeezed state, while the signal and idler modes each contain  $n_s$  and  $n_i$  photons respectively, as shown in Fig. 1(a). We denote this three-mode quantum state as  $|n_p, n_i, n_s\rangle$  for convenience. Since the Hamiltonian Eq. (2) commutes with the observables  $a_p^\dagger a_p + a_s^\dagger a_s$  and  $a_i^\dagger a_i - a_s^\dagger a_s$ , we introduce two conserved quantities

$$\begin{aligned} N &= n_p + n_s, \\ M &= n_i - n_s, \end{aligned} \quad (4)$$

for a three-mode Fock-state input  $|n_p, n_i, n_s\rangle$ . These two conserved quantities are the analogs of Manley-Rowe relations [45] from classical nonlinear optics, reflecting the fact that, without considering the dissipation and any other energy injection, the total photon number of pump and signal modes and the number difference between signal and idler modes are invariants.

The conserved quantities in Eq. (4) ensure that the photon number in pump, signal, and idler modes are completely correlated. Consequently, the system will evolve in the subspace spanned by

$$\{|N - n, M + n, n\rangle \mid N \geq n \geq \max(0, -M)\}. \quad (5)$$

Without loss of generality, we assume  $M > 0$ , and then the output state can be written as

$$|\psi(\kappa t)\rangle = \sum_{n=0}^N c_n(\kappa t) |N - n, M + n, n\rangle. \quad (6)$$

The Hamiltonian given in Eq. (2) can then be expanded in detail in the associated subspace spanned by Eq. (5).

### III. FOCK-STATE ENCODING FOR QUANTUM SIMULATIONS

In an analog quantum simulation, we need to formally map the Hamiltonian to be solved to our controllable Hamiltonian [15], i.e., the nonlinear Hamiltonian presented in Eq. (2). Because the evolution time  $t$  and coupling coefficient  $\kappa$  have the same status in the time-evolution operator Eq. (3),

we combine them into one parameter and rewrite the time-evolution operator as

$$U(\kappa t) = e^{-i\kappa t H_{\text{NL}}}, \quad (7)$$

with the rescaled nonlinear Hamiltonian

$$H_{\text{NL}} = a_p a_s^\dagger a_i^\dagger + a_p^\dagger a_s a_i. \quad (8)$$

There are commonly used methods for mapping boson creation and annihilation operators onto spin operators, e.g., the Holstein-Primakoff transformation [46] and the Jordan-Schwinger transformation [47,48]. However, these transformations have limitations in their applicability to certain types of bosonic systems. Specifically, they are not directly applicable to the full quantum treatment of  $\chi^{(2)}$  nonlinearity, i.e., Hamiltonian Eq. (8), which involves a bosonic system with three different bosonic modes and third-order term. To achieve quantum simulation, we explicitly expand  $H_{\text{NL}}$  into formal mathematical matrix in the subspace spanned by Eq. (5). The matrix element  $[H_{\text{NL}}]_{ij}^{\text{Fock}}$ , defined as  $\langle N - i, M + i, i | H_{\text{NL}} | N - j, M + j, j \rangle$ , satisfies

$$\begin{aligned} [H_{\text{NL}}]_{ij}^{\text{Fock}} &= \sqrt{i(N+1-i)(M+i)} \delta_{i,j-1} \\ &\quad + \sqrt{j(N+1-j)(M+j)} \delta_{i-1,j}, \end{aligned} \quad (9)$$

where  $\delta_{i,j}$  is the Kronecker delta function,  $\delta_{i,j} = 1$  for  $i = j$ , and  $\delta_{i,j} = 0$  otherwise. Accordingly, the Hamiltonian  $H_{\text{NL}}$  has the matrix representation

$$\begin{aligned} &[H_{\text{NL}}]^{\text{Fock}} \\ &= \begin{pmatrix} 0 & \sqrt{N(M+1)} & \cdots & 0 & 0 \\ \sqrt{N(M+1)} & 0 & \cdots & 0 & 0 \\ \vdots & \vdots & \ddots & \vdots & \vdots \\ 0 & 0 & \cdots & 0 & \sqrt{N(M+N)} \\ 0 & 0 & \cdots & \sqrt{N(M+N)} & 0 \end{pmatrix}, \end{aligned} \quad (10)$$

which is a tridiagonal matrix with zero diagonal elements. The tridiagonality arises from the Hamiltonian guiding the evolution of a pump photon converting to a signal-idler photon pair and the inverse. Therefore, the dynamic of a tree-mode Fock state  $|N - n, M + n, n\rangle$  is only related to the states whose number of photons differs by 1 in each mode, i.e.,  $|N - (n + 1), M + (n + 1), n + 1\rangle$ , and  $|N - (n - 1), M + (n - 1), n - 1\rangle$ . Actually, tridiagonal Hamiltonians were used to describe several one-dimensional systems [49–51], inspiring us to map the nonlinear Hamiltonian  $H_{\text{NL}}$  to a one-dimensional system.

Now we will show that a Hamiltonian in such a form can be directly mapped to the one describing a general chiral  $XY$  spin-1/2 chain, which can be used to study phenomena such as many-body-localization [52] and dynamic phase transitions [53], in the single excitation subspace spanned by the states

$$|j\rangle = |\downarrow_1 \downarrow_2 \cdots \downarrow_{j-1} \uparrow_j \downarrow_{j+1} \cdots \downarrow_L\rangle, \quad (11)$$

with  $L$  standing for the length of the spin chain and  $j = 1, 2, \dots, L$  marking the position of the excitation, as shown in Fig. 1(b). The mathematical description of the Hamiltonian

describing a general chiral  $XY$  spin-1/2 chain is given as

$$H_{XY} = \sum_{n=1}^N \frac{J_n}{2} (\sigma_n^x \sigma_{n+1}^x + \sigma_n^y \sigma_{n+1}^y), \quad (12)$$

where  $\sigma_n^x$  and  $\sigma_n^y$  are the Pauli operators of the spin at the  $n$ th site and  $J_n$  represents the couplings between  $n$ th and  $(n+1)$ th spin. It can also be rewritten in terms of the raising and lowering operators as

$$H_{XY} = \sum_{n=1}^N J_n (\sigma_n^+ \sigma_{n+1}^- + \sigma_n^- \sigma_{n+1}^+), \quad (13)$$

with  $\sigma_n^\pm = \frac{1}{2}(\sigma_n^x \pm i\sigma_n^y)$ , satisfying

$$\sigma_n^+ |0\rangle = |n\rangle, \quad \sigma_n^- |n\rangle = |0\rangle, \quad (14)$$

with  $|0\rangle$  standing for the all-spin-down state  $|\downarrow_1, \dots, \downarrow_L\rangle$ . Accordingly, in the single excitation subspace, the Hamiltonian  $H_{XY}$  has a explicit matrix form

$$[H_{XY}]^{\text{Spin}} = \begin{pmatrix} 0 & J_1 & 0 & \cdots & 0 & 0 \\ J_1 & 0 & J_2 & \cdots & 0 & 0 \\ 0 & J_2 & 0 & \cdots & 0 & 0 \\ \vdots & \vdots & \vdots & \ddots & \vdots & \vdots \\ 0 & 0 & 0 & \cdots & 0 & J_N \\ 0 & 0 & 0 & \cdots & J_N & 0 \end{pmatrix}, \quad (15)$$

with the matrix elements giving as  $[H_{XY}]_{ij}^{\text{Spin}} = \langle i | H_{XY} | j \rangle = J_{j-1} \delta_{j,i+1} + J_{i-1} \delta_{i,j+1}$ . Comparing Eqs. (10) and (15), it can be obviously find that  $[H_{\text{NL}}]^{\text{Fock}}$  exactly equals  $[H_{XY}]^{\text{Spin}}$  if we set the couplings of spin chain as

$$J_n = \sqrt{n(N+1-n)(M+n)}. \quad (16)$$

The coupling  $J_n$  shows that the interaction strength is not only related to  $N$ , which is determined given a specific chain length  $L$ , but also regulated by  $M$ . The parameter  $M$  extends the range of Hamiltonian that can be simulated and improves the capability of the simulator.

The correspondence  $[H_{XY}]^{\text{Spin}} = [H_{\text{NL}}]^{\text{Fock}}$  specifies a one-to-one mapping between the three-mode Fock states of a optical system and the single excitation states of a spin chain,  $|N-n, M+n, n\rangle \leftrightarrow |n+1\rangle$ . The length of the spin chain is limited by the total photons in the pump and signal modes, while the photons in the idler mode can be regarded as an ancilla providing the variable site-dependent couplings involved in the spin chain.

Our simulator is not limited to the single excitation of an  $XY$  spin chain. By using the Jordan-Wigner transformation, it can simulate a fermionic system governed by a generalized nonlinear SSH Hamiltonian [54] that belongs to the chiral orthogonal class of Altland-Zirnbauer symmetry classes [55]. Furthermore, mapping to the Bogoliubov-de Gennes Hamiltonians [56] allows us to simulate the Kitaev model [57] and the transverse-field Ising model. Although similar simulations can be implemented in a linear optical simulator, the nonlinearity in our simulation scheme provides additional simulation parameters. Table I lists a comparison between our simulation scheme and a linear optical simulator.

TABLE I. The comparison between the nonlinear optical systems and linear optical systems.

System	Nonlinear optics	Linear optics <sup>a</sup>
Hamiltonian	$H_{\text{NL}} = a_p a_s^\dagger a_i^\dagger + a_p^\dagger a_s a_i$	$H_{\text{BS}} = a^\dagger b + b^\dagger a$
Conservation	$N = a_p^\dagger a_p + a_s^\dagger a_s;$ $M = a_i^\dagger a_i - a_s^\dagger a_s$	$S = a^\dagger a + b^\dagger b$
State	$ N-n\rangle_p  M+n\rangle_i  n\rangle_s$	$ l\rangle_a  S-l\rangle_b$
Simulated Hamiltonian	$H_{XY} = \sum_{n=1}^{L-1} \frac{J_n}{2} (\sigma_n^x \sigma_{n+1}^x + \sigma_n^y \sigma_{n+1}^y)$	
System size $L$	$N+1$	$S+1$
Interaction strength $J_n$	$\sqrt{n(N+1-n)(M+n)}$ (relatively adjusted by $M$ )	$\sqrt{n(S+1-n)}$
Relation	$H_{\text{NL}}$ degenerates to $H_{\text{BS}}$ while $M \rightarrow \infty$ .	

<sup>a</sup>Reference [32].

#### IV. SOLVING THE PHOTON NUMBER STATISTICS

Now that the spin state was encoded in the multimode Fock states in a nonlinear quantum optical system, solving the dynamics of the spin precisely means tracing the time evolution of the number state governed by the nonlinear Hamiltonian  $H_{\text{NL}}$ . Obviously,  $H_{\text{NL}}$  can be diagonalized as

$$H_{\text{NL}} = T \Lambda T^\dagger, \quad (17)$$

with  $T$  a unitary matrix diagonalizing matrix  $[H_{\text{NL}}]^{\text{Fock}}$  and  $\Lambda = \text{diag}(\lambda_1, \lambda_2, \dots, \lambda_{N+1})$  the eigenvalues of  $[H_{\text{NL}}]^{\text{Fock}}$ . The time-evolution operator in Eq. (7) can then be expressed in a computation-friendly form  $U(\kappa t) = T \exp(-i\kappa t \Lambda) T^\dagger$ . Consequently, with an input state  $|N-n, M+n, n\rangle$ , the superposition coefficients of time-evolved states in Eq. (6) are the matrix elements of  $U(\kappa t)$ ,

$$c_{n'}(\kappa t) = \langle N-n', M+n', n' | U(\kappa t) | N-n, M+n, n \rangle = [T \exp(-i\kappa t \Lambda) T^\dagger]_{n'n}. \quad (18)$$

Using these coefficients we can further characterize the time evolution of the photon number distribution during the nonlinear process.

Since the conservation given in Eq. (4), the photon number distribution of three optical modes can be further simplified to single-mode. We chose the signal photon number distribution  $P(n, \kappa t) = |c_n(\kappa t)|^2$  to describe the evolution of the entire system. Four examples of  $P(n, \kappa t)$  are shown in Figs. 2(a) to 2(d), with input states  $|50, 1, 0\rangle$ ,  $|50, 10, 0\rangle$ ,  $|50, 50, 0\rangle$ ,  $|50, 100, 0\rangle$ , respectively, together with the corresponding average signal photon number  $\langle n \rangle = \sum_{n=0}^N n P(n, \kappa t)$  and the second-order autocorrelation function  $g^{(2)}(0)$  in Figs. 2(e) to 2(h).

In all four examples, the distribution of the signal photon number shows oscillatory behavior, indicating a competition between two process in the nonlinear process: down-conversion, where pump photons generate pairs of signal and idler photons, and its reverse, known as the sum frequency. Such oscillatory behavior is not observed in the semi-classical treatment where the down-conversion process is dominant due to the strong pump light. The difference between

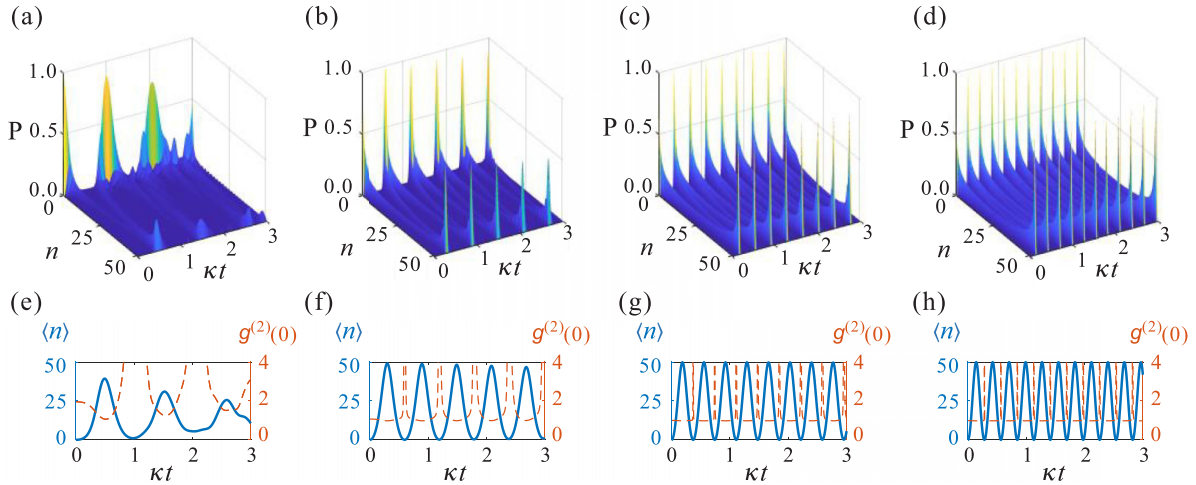


FIG. 2. The photon number statistics during the nonlinear process. (a)–(d) The signal photon number distribution  $P$  as a function of time  $\kappa t$ , with initial state  $|50, M, 0\rangle$  for (a)  $M = 1$ , (b)  $M = 10$ , (c)  $M = 50$ , (d)  $M = 100$ . (e)–(h) The corresponding mean signal photon number  $\langle n \rangle$  (blue solid line) and autocorrelation function  $g^{(2)}(0)$  (red dashed line) as a function of  $\kappa t$ , with initial state  $|50, M, 0\rangle$  for (e)  $M = 1$ , (f)  $M = 10$ , (g)  $M = 50$ , (h)  $M = 100$ .

semi-classical and full quantum treatment is also reflected in  $g^2(0)$ . The semi-classical treatment gives a prediction of  $g^2(0) = 1 + \frac{1}{M}$ , consistent with the results obtained by full-quantum methods when  $\kappa t \ll 1$ , but  $g^2(0)$  varies with  $\kappa t$  since the variation of the photon number in the pump mode cannot be ignored in the full-quantum treatment.

To quantitatively investigate the oscillation behavior, we examine the frequency domain by calculating the Fourier transform  $\langle \tilde{n} \rangle(f) = \mathcal{F}[\langle n \rangle(\kappa t)]$  where  $\mathcal{F}[*]$  denotes the Fourier transform. The results are shown in Fig. 3(a). The spectrum depends on the value of  $M$ , indicating that the energy spectral structure of the Hamiltonian changes

with  $M$ , thus demonstrating the adjustability of coupling strength during the simulation. This suggests that our simulator has superior simulation capabilities compared to a linear simulator, such as the one used in the previous studies. Furthermore, as shown in Fig. 3(a), the width of  $\langle \tilde{n} \rangle(f)$  decreases as  $M$  increases, which means the oscillation becomes more and more harmonic. We define  $f_m$  as the principal frequency, which is the frequency at which  $\langle \tilde{n} \rangle(f)$  takes the maximum value, to characterize the oscillation rate. In fact, these peaks correspond to the differences between eigenfrequencies. In the Fig. 3(a), we draw the lowest eigenfrequencies of the systems with different  $M$  using dashed lines. These dashed lines bound the lower limit of peak values. We notice that the peak

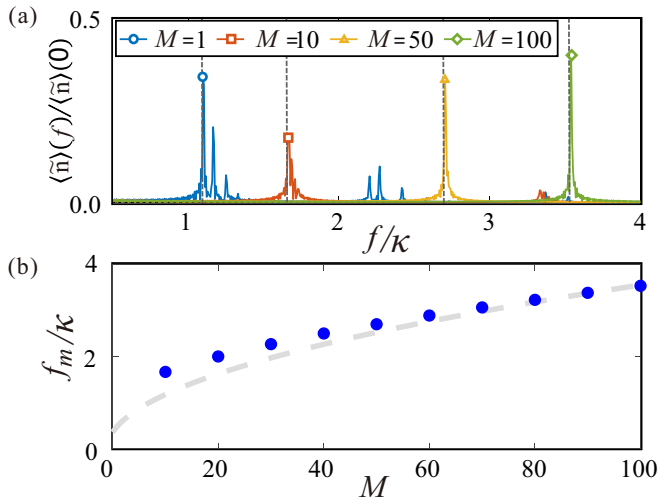


FIG. 3. The signal photon number oscillation in frequency space. (a) The frequency distribution of signal photon number oscillation with  $M = 1$  (blue),  $M = 10$  (red),  $M = 50$  (yellow), and  $M = 100$  (green), the dashed lines are corresponding lowest eigenfrequencies. (b) The principal frequency component of signal photon number oscillation with  $M$  from 10 to 100. The dashed line is a visual guide  $\propto \sqrt{M + 1}$ .

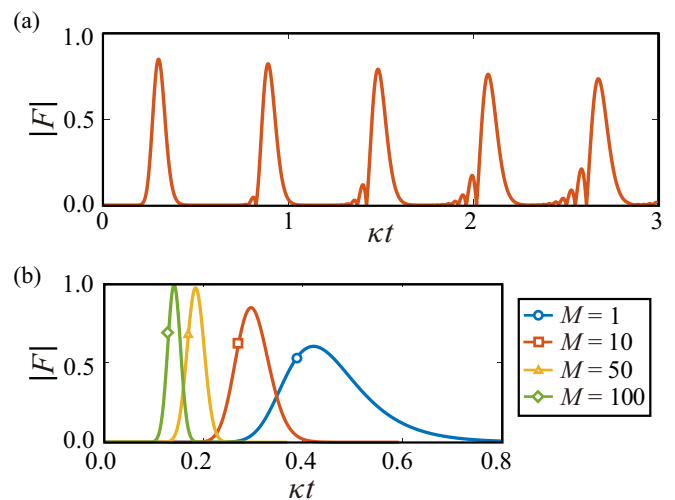


FIG. 4. The absolute value of overlap  $F$  in Eq. (19). (a) The curve of the  $|F|$  varying with simulation duration  $\kappa t$  has periodic peaks, the initial state is  $|50, 10, 0\rangle$ . (b) The  $|F|$  for different initial states  $|50, M, 0\rangle$ , with  $M = 1$  (blue), 10 (red), 50 (yellow), 100 (green), respectively, simulation duration  $\kappa t$  is limited in first peak of the  $|F|$  for visual clarity.

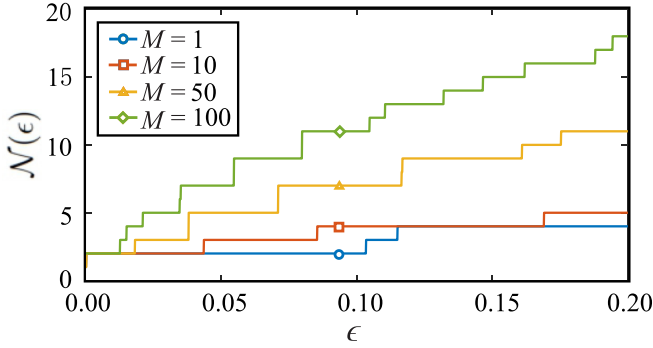


FIG. 5. The maximal number of energy gaps in energy interval of width  $\epsilon$ , denoted as  $\mathcal{N}(\epsilon)$ , of the simulated Hamiltonian  $H_{XY}$  with coupling in Eq. (16) for  $N = 50$ ,  $M = 1$  (blue),  $M = 10$  (red),  $M = 50$  (yellow),  $M = 100$  (green).

value is slightly larger than the lowest eigenfrequency, which can be attributed to the influence of the peaks corresponding to higher frequencies. As shown in Fig. 3(b),  $f_m$  increases with  $M$ , and is proportional to  $\sqrt{M+1}$  if  $M \gg N$ , which means the signal photon number oscillates faster when the idler photon number input increases. In other words, the idler photons enhance the nonlinear process.

## V. STATE TRANSFER ON THE SPIN CHAIN

The transfer of arbitrary quantum states across a network is a key aspect of quantum information processing and has been extensively studied in the one-dimensional situation [58–61]. In such cases, a one-dimensional network can be modeled as a chain with  $L$  sites, each of which contains a spin-1/2. Initially, the spin on the first site is prepared in a superposition of the two spin eigenstates,  $\alpha|\downarrow\rangle + \beta|\uparrow\rangle$ , while all other spins prepared in  $|\downarrow\rangle$ . Recalling the single excitation state

$|j\rangle$  in Eq. (11) and the all-spin-down state  $|0\rangle$ , the initial state of the spin chain reads  $(\alpha|\downarrow\rangle + \beta|\uparrow\rangle)_1|\downarrow_2, \dots, \downarrow_L\rangle = \alpha|0\rangle + \beta|1\rangle$ . Our purpose is evolving it into the target state  $|\downarrow_1, \dots, \downarrow_{L-1}\rangle(\alpha|\downarrow\rangle + \beta|\uparrow\rangle)_L = \alpha|0\rangle + \beta|L\rangle$  via the nearest-neighbor interactions on the spin chain. Both the initial and target states are in the superposition of the state  $|0\rangle$  and one of the single excitation states  $|j\rangle$  with the same superposition coefficients  $\alpha, \beta$ . Since the state  $|0\rangle$  remains unchanged under the  $XY$  interaction, we can focus on the single-excitation subspace in which our simulation scheme operates. It is worth noting that the perfect state transfer only occurs for certain couplings. For instance, perfect state transfer happens if we set the coupling  $J_n \propto \sqrt{n(N+1-n)}$  in Eq. (12) [59]. As mentioned in Sec. III, the coupling of the simulated spin chain can be adjusted by  $M$ , hence we can study the state transfer quality of different couplings by changing  $M$ . Importantly, our simulator can achieve perfect state transfer if  $M \gg N$ . We use the overlap between the state  $|1\rangle$  after time evolution and the state  $|L\rangle$  to quantify the transfer quality

$$F = \langle L|e^{-iH}|1\rangle, \quad (19)$$

with  $H$  the Hamiltonian of spin chain and  $t$  the transfer time.  $|F| = 1$  indicates a perfect state transfer.

In previous works, state transfer of a one-dimensional spin chain was simulated using photons on a multiphoton linear interference network [32] and an integrated photonic chip [62]. The previous approach used high photon number Fock states to implement a long spin-chain simulation, but lost the adjustability of couplings and can only simulate perfect state transfer situations. The later approach allowed for easy tuning of spin couplings but was difficult to scale up, as simulating  $N$  spins requires at least  $N$  waveguides. Our protocol takes advantage of both approaches, where the input parameters  $N$  and  $M$  control the length and relative coupling strength of the simulated spin chain, respectively.

The simulation of state transfer follows a specific procedure. First, the chain length  $L$  to be simulated is determined and  $M$  is chosen to determine the coupling of the simulated spin chain. Next, the three-mode Fock state  $|L-1, M, 0\rangle$  is prepared as the simulator's input and the coupling coefficient  $\kappa$  is adjusted to control the simulation duration. Finally, the photon distribution of the output signal mode is measured and the quality of state transfer is determined by the probability  $P(L-1, \kappa t) = |F|^2$ .

Our first study kept the chain length  $L = 51$  and varied  $M$  from 0 to 100. Figure 4(a) shows a typical curve of  $|F|$  as a function of simulation duration  $\kappa t$ . The curve exhibits periodic peaks, which decrease in height as the duration increases, consistent with the photon number statistics results presented in Sec. IV. The oscillatory behavior of the signal in nonlinear optics causes the excitation to oscillate back and forth between the two ends of the chain, leading to periodic peaks in the  $|F|$  values. However, the accumulated transfer errors in each round trip cause a gradual decrease in the peak height. To demonstrate the effect of  $M$  on transfer quality, we plot four curves of  $|F|$  with  $M = 1, 10, 50, 100$  in Fig. 4(b). The maximum values of  $|F|$  appear earlier for larger values  $M$ , which is consistent with the mean photon number oscillation rate shown in Fig. 3. Moreover, the maximum value of  $|F|$

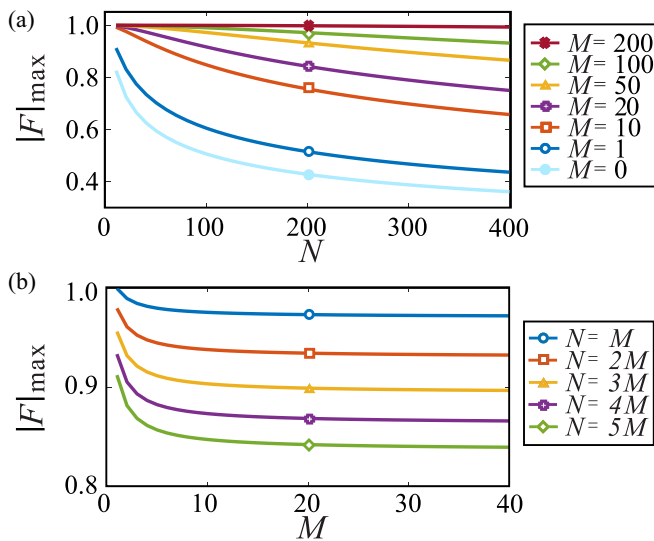


FIG. 6. The transfer quality of different simulation setups. (a) The maximum overlap  $|F|_{\max}$  as function of input parameter  $N$  with a fixed  $M$ . (b) The maximum overlap  $|F|_{\max}$  as a function of  $M$  with fixed  $N/M$  ratio.

tends to 1 as  $M$  increases, indicating better state transfer quality.

From a thermodynamic point of view, the decay of the  $|F|$  is related to the equilibration on average of rank-one observable  $|\underline{L}\rangle\langle\underline{L}|$  whose timescale has a strong dependency on the degeneracy of energy gaps [63]. To quantify the degeneracy, in Ref. [64] the maximal number of energy gaps in the energy interval of width  $\epsilon$  was defined as

$$\mathcal{N}(\epsilon) = \max_E |\{(k, l) : k \neq l \text{ and } G_{k,l} \in [E, E + \epsilon]\}|, \quad (20)$$

where  $G_{k,l} = \lambda_k - \lambda_l$  is the energy gap between the  $k$ th and  $l$ th eigenstates. The equilibration on average is expected to happen on a timescale  $1/\epsilon$  for  $\mathcal{N}(\epsilon)$ , which is small compared to  $d_{\text{eff}}$ , the effective dimension of the initial state, defined as

$$d_{\text{eff}} = \frac{1}{\sum_n |\langle \psi_n | \psi(0) \rangle|^4}, \quad (21)$$

where  $|\psi_n\rangle$  stands for  $n$ th eigenstate of the Hamiltonian and  $|\psi(0)\rangle$  is the initial state. In the example,  $|\psi(0)\rangle = |\underline{1}\rangle$ , and  $d_{\text{eff}} = 4.8, 7.8, 10.5, 11.3$  for  $M = 1, 10, 50, 100$ , respectively.

Therefore, one of the reasonable requirements for perfect state transfer, which is a nonequilibrium process, is a uniform energy gap, leading to an infinite time for equilibration on average. Trying to find the underlying mechanism, we plot  $\mathcal{N}(\epsilon)$  for the simulated Hamiltonian with different  $M$  in Fig. 5. The energy gaps of the simulated Hamiltonian have a flatter distribution as  $M$  increases, thus  $\mathcal{N}(\epsilon)$  grows faster with  $\epsilon$ . We chose  $\mathcal{N}(\epsilon) = 2$  as the judging standard because it is the smallest possible  $\mathcal{N}(\epsilon)$ .  $\mathcal{N}(\epsilon) = 2$  as long as  $\epsilon < 0.104, 0.044, 0.018, 0.013$  for  $M = 1, 10, 50, 100$ , respectively, with the corresponding  $|F| = 0.604, 0.847, 0.9720, 0.990$ . As expected, the transfer quality improves with the energy gaps being flat.

To further explore the relationship between the quality of the state transfer and equilibrium on average of the observable, we observe how  $|F|$  changes with simulated chain length  $N + 1$ , as the time it takes for the system to reach equilibrium is closely related to the system size. Figure 6(a) shows the  $|F|_{\text{max}}$  of different  $(N, M)$  input combinations. As expected, longer simulated chains have lower transfer quality with a fixed  $M$  because larger systems tend to reach local equilibrium more quickly. Additionally, transfer quality increases with  $M$ , regardless of chain length, which is consistent with previous findings. It is a nontrivial problem to examine how transfer quality changes when two competing factors,  $N$  and  $M$ , increase simultaneously. Figure 6(b) shows that  $|F|_{\text{max}}$  tends to be constant as the simulated chain length increases while keeping the  $N/M$  ratio. The transfer quality at the thermodynamic limit is strongly influenced by the  $N/M$  ratio and the smaller the  $N/M$  ratio, the better the asymptotic transfer quality.

## VI. DISCUSSION

Our proposed method can be extended to nonlinear processes with higher-order nonlinearity as well as multimode scenarios. One possible extension is to employ spectral degrees of freedom during the nonlinear process and apply a Schmidt decomposition to reduce the continuous frequency

freedom into an effectively discrete space [65]. The effective dimension can be further controlled by spectral engineering [66,67]. Although adding more mode numbers obviously increases the complexity of the simulator, how to enhance the simulation capabilities in the presence of the multimode remains an open question. Nevertheless, our approach shows promise for simulating problems that exhibit quantum superiority by increasing the number of modes, such as Boson sampling [30], which considers the distribution of photons after scattering. When taking into account the rich degrees of freedom of the three interacting waves inside the nonlinear crystal, discussions of quantum superiority may become possible, and this is an area of further research interest for us.

To implement our proposal experimentally, there are difficulties in three aspects: generating the high-order Fock states in pump and idler modes; implementing sufficiently high and adjustable nonlinear strength; finally, the photon-number-resolving detection in the output. While these challenges may seem daunting, the scientific community is working diligently to overcome them and there have been significant advancements in relevant techniques. We will briefly review some of these techniques to demonstrate how we can address the challenges we face.

Generally, preparing a multiphoton state can be on-demand by using atoms [68] or quantum dots [69] or heralded by using optical parametric process [70]. Currently, the number of photons in a high-order Fock state can approach 7 using atoms [71] and 5 using quantum dots [72]. Recently, Silberhorn and colleagues showed that spontaneous parametric down-conversion (SPDC) has sufficient potential to generate the heralded higher-order Fock state, for the 50-photon event happens about twice per second with a PDC mean photon number of 7 [73]. Their subsequent work found that Fock states with  $n = 9$  could be generated at 0.1 Hz with high fidelity under current experimental constraints [74]. The number of photons generated can be further enhanced at the expense of generation rate. In addition to probabilistic generation via SPDC, there are also other on-demand methods. By employing a two-level atom resonantly interacting with a coherent state, one could generate Fock states as large as  $n = 50$  with a fidelity of 58% in a cavity QED setup [75], and the number of photons in a Fock state could be further increased to 100 in the near future by reducing decoherence.

Another difficulty in experimentally demonstrating our proposal is improving the nonlinear strength, which determines the simulation duration. Actually, a long-standing goal in optical science has been the implementation of nonlinear effects at progressively lower light powers or pulse energy [8]. That implies the entire community has been trying to achieve large nonlinearities all the time, mainly along three routes. Nowadays, there have been some significant advances in all of them. The first is the natural idea of looking for new materials or structures with high nonlinear coefficients. As reviewed in detail in Ref. [76], plasmonic metasurfaces can contribute “significantly to the control of optical nonlinearity and enhancement of nonlinear generation efficiency.” The second method is focusing the photons both spatially and temporally to achieve a high collision probability. This can lead to an increase in the power density of the light, which can, in turn, make the nonlinear effect more pronounced [77].

Third, optical cavities can be added to increase the number of times the photons interact with each other, thereby enhancing the nonlinear effect. Strong light-matter interactions are crucial for this approach and efforts to achieve this go back to 1987, when a microcavity with a single Rydberg atom was used to demonstrate strong coupling [78]. Subsequent improvements focused on increasing the quality of the cavity and changing the medium inside the cavity. A recent work reported an “ultra-high-quality ( $Q$  up to  $10^8$ ) doped microcavity” employing thulium, erbium, and ytterbium elements corporately [79]. To achieve the required nonlinear strength for our scheme, enhancing the nonlinear effect with an optical cavity is the most promising approach. This argument is supported by previous peer publications. For example, in Ref. [7], the authors proposed an optical quantum computation scheme based on second-order nonlinearities, which required cavities with  $Q \sim 2 \times 10^8$  to enhance nonlinearity. Similarly, the authors of Ref. [80] discussed a deterministic  $N$ -photon-state generation proposal using the same Hamiltonian, which also required cavities with  $Q \sim 3 \times 10^8$ . Despite the current limitations in cavity fineness, the authors still discussed these proposals in theory because such high- $Q$  cavities are believed to be achievable in principle [81]. Our quantum simulation scheme requires nonlinear strength at the same order of magnitude.

The commonly used photon-number resolving detection methods include transition edge sensors (TES) and multiplexed threshold detectors. Recently, by multiplexing 16 TESs temporally and spatially, researchers were able to register events with up to 219 photons, with each TES having intrinsic photon number resolving ability up to 5 with high fidelity [82]. Multiplexing highly quantum-efficient TESs to accurately resolve photon numbers between 0 and 100 was also achieved in an experiment for implementing a quantum random-number generator with no inherent bias [83]. Besides the TES approach, spatiotemporally multiplexing threshold

detectors can also provide photon number-resolving ability. A recent breakthrough in this area comes from Tang’s group at Yale University who developed an on-chip detector that can resolve up to 100 photons by spatiotemporally multiplexing an array of superconducting nanowires along a single optical waveguide [84]. Moreover, new data analysis methods are also improving the resolution of photon number detection. In Ref. [85], “a measurement workflow free of systematic errors consisting of a reconfigurable photon number-resolving detector, custom electronic circuitry, and a faithful data-processing algorithm” was reported. With this tool, the authors achieved an “unprecedented accurate measurement” with an average fidelity of 0.998. These recent advancements in both hardware and data analysis methods suggest that photon number resolution detection capabilities will continue to improve and fulfill the requirements in many applications, including those outlined in our proposal.

In summary, although our proposed scheme for quantum simulation using photon number resolving detectors and strong nonlinear effects may face some experimental challenges at present, they are not insurmountable obstacles and are more likely technical issues that can be resolved with continued research and development.

#### ACKNOWLEDGMENTS

This work was supported by the Innovation Program for Quantum Science and Technology (Grant No. 2021ZD0301200), the National Natural Science Foundation of China (Grants No. 12022401, No. 62075207, No. 11874343, No. 11821404, and No. 12204468), the Fundamental Research Funds for the Central Universities (Grants No. WK2470000026 and No. WK2470000030), the CAS Youth Innovation Promotion Association (Grant No. 2020447), and the Anhui Initiative in Quantum Information Technologies (Grant No. AHY020100).

- 
- [1] F. Flamini, N. Spagnolo, and F. Sciarrino, Photonic quantum information processing: a review, *Rep. Prog. Phys.* **82**, 016001 (2019).
  - [2] E. Knill, R. Laflamme, and G. J. Milburn, A scheme for efficient quantum computation with linear optics, *Nature (London)* **409**, 46 (2001).
  - [3] P. Kok, W. J. Munro, K. Nemoto, T. C. Ralph, J. P. Dowling, and G. J. Milburn, Linear optical quantum computing with photonic qubits, *Rev. Mod. Phys.* **79**, 135 (2007).
  - [4] I. L. Chuang and Y. Yamamoto, Simple quantum computer, *Phys. Rev. A* **52**, 3489 (1995).
  - [5] N. K. Langford, S. Ramelow, R. Prevedel, W. J. Munro, G. J. Milburn, and A. Zeilinger, Efficient quantum computing using coherent photon conversion, *Nature (London)* **478**, 360 (2011).
  - [6] M. Y. Niu, I. L. Chuang, and J. H. Shapiro, Qudit-Basis Universal Quantum Computation using  $\chi^{(2)}$  Interactions, *Phys. Rev. Lett.* **120**, 160502 (2018).
  - [7] S. Krastanov, M. Heuck, J. H. Shapiro, P. Narang, D. R. Englund, and K. Jacobs, Room-temperature photonic logical qubits via second-order nonlinearities, *Nat. Commun.* **12**, 191 (2021).
  - [8] D. E. Chang, V. Vuletić, and M. D. Lukin, Quantum nonlinear optics—photon by photon, *Nat. Photonics* **8**, 685 (2014).
  - [9] J. Lu, M. Li, C.-L. Zou, A. A. Sayem, and H. X. Tang, Toward 1% single-photon anharmonicity with periodically poled lithium niobate microring resonators, *Optica* **7**, 1654 (2020).
  - [10] M. Placke and S. Ramelow, Engineering algaas-on-insulator toward quantum optical applications, *Opt. Lett.* **45**, 6763 (2020).
  - [11] S. Ramelow, A. Farsi, Z. Vernon, S. Clemmen, X. Ji, J. E. Sipe, M. Liscidini, M. Lipson, and A. L. Gaeta, Strong Nonlinear Coupling in a  $\text{Si}_3\text{N}_4$  Ring Resonator, *Phys. Rev. Lett.* **122**, 153906 (2019).
  - [12] M. Heuck, K. Jacobs, and D. R. Englund, Photon-photon interactions in dynamically coupled cavities, *Phys. Rev. A* **101**, 042322 (2020).
  - [13] A. W. Bruch, X. Liu, J. B. Surya, C.-L. Zou, and H. X. Tang, On-chip  $\chi^{(2)}$  microring optical parametric oscillator, *Optica* **6**, 1361 (2019).
  - [14] T. P. McKenna, H. S. Stokowski, V. Ansari, J. Mishra, M. Jankowski, C. J. Sarabalis, J. F. Herrmann, C. Langrock, M. M. Fejer, and A. H. Safavi-Naeini, Ultra-low-power second-order nonlinear optics on a chip, *Nat. Commun.* **13**, 4532 (2022).

- [15] I. M. Georgescu, S. Ashhab, and F. Nori, Quantum simulation, *Rev. Mod. Phys.* **86**, 153 (2014).
- [16] R. Blatt and C. F. Roos, Quantum simulations with trapped ions, *Nat. Phys.* **8**, 277 (2012).
- [17] C. Monroe, W. C. Campbell, L.-M. Duan, Z.-X. Gong, A. V. Gorshkov, P. W. Hess, R. Islam, K. Kim, N. M. Linke, G. Pagano, P. Richerme, C. Senko, and N. Y. Yao, Programmable quantum simulations of spin systems with trapped ions, *Rev. Mod. Phys.* **93**, 025001 (2021).
- [18] C. Gross and I. Bloch, Quantum simulations with ultracold atoms in optical lattices, *Science* **357**, 995 (2017).
- [19] F. Schäfer, T. Fukuhara, S. Sugawa, Y. Takasu, and Y. Takahashi, Tools for quantum simulation with ultracold atoms in optical lattices, *Nat. Rev. Phys.* **2**, 411 (2020).
- [20] A. A. Houck, H. E. Türeci, and J. Koch, On-chip quantum simulation with superconducting circuits, *Nat. Phys.* **8**, 292 (2012).
- [21] K. Xu, Z.-H. Sun, W. Liu, Y.-R. Zhang, H. Li, H. Dong, W. Ren, P. Zhang, F. Nori, D. Zheng *et al.*, Probing dynamical phase transitions with a superconducting quantum simulator, *Sci. Adv.* **6**, eaba4935 (2020).
- [22] A. Aspuru-Guzik and P. Walther, Photonic quantum simulators, *Nat. Phys.* **8**, 285 (2012).
- [23] X.-S. Ma, B. Dakic, W. Naylor, A. Zeilinger, and P. Walther, Quantum simulation of the wavefunction to probe frustrated heisenberg spin systems, *Nat. Phys.* **7**, 399 (2011).
- [24] A. Schreiber, A. Gábris, P. P. Rohde, K. Laiho, M. Štefaňák, V. Potoček, C. Hamilton, I. Jex, and C. Silberhorn, A 2d quantum walk simulation of two-particle dynamics, *Science* **336**, 55 (2012).
- [25] T. Kitagawa, M. A. Broome, A. Fedrizzi, M. S. Rudner, E. Berg, I. Kassal, A. Aspuru-Guzik, E. Demler, and A. G. White, Observation of topologically protected bound states in photonic quantum walks, *Nat. Commun.* **3**, 882 (2012).
- [26] J.-S. Xu, K. Sun, Y.-J. Han, C.-F. Li, J. K. Pachos, and G.-C. Guo, Simulating the exchange of majorana zero modes with a photonic system, *Nat. Commun.* **7**, 13194 (2016).
- [27] L. Xiao, X. Zhan, Z. Bian, K. Wang, X. Zhang, X. Wang, J. Li, K. Mochizuki, D. Kim, N. Kawakami *et al.*, Observation of topological edge states in parity-time-symmetric quantum walks, *Nat. Phys.* **13**, 1117 (2017).
- [28] F. Cardano, A. D'Errico, A. Dauphin, M. Maffei, B. Piccirillo, C. de Lisio, G. De Filippis, V. Cataudella, E. Santamato, L. Marrucci *et al.*, Detection of zak phases and topological invariants in a chiral quantum walk of twisted photons, *Nat. Commun.* **8**, 15516 (2017).
- [29] X.-Y. Xu, Q.-Q. Wang, W.-W. Pan, K. Sun, J.-S. Xu, G. Chen, J.-S. Tang, M. Gong, Y.-J. Han, C.-F. Li, and G.-C. Guo, Measuring the Winding Number in a Large-Scale Chiral Quantum Walk, *Phys. Rev. Lett.* **120**, 260501 (2018).
- [30] S. Aaronson and A. Arkhipov, *Proceedings of the Forty-Third Annual ACM Symposium on Theory of Computing* (ACM, New York, 2011), pp. 333–342.
- [31] H.-S. Zhong, H. Wang, Y.-H. Deng, M.-C. Chen, L.-C. Peng, Y.-H. Luo, J. Qin, D. Wu, X. Ding, Y. Hu *et al.*, Quantum computational advantage using photons, *Science* **370**, 1460 (2020).
- [32] T. Sturges, T. McDermott, A. Buraczewski, W. Clements, J. Renema, S. Nam, T. Gerrits, A. Lita, W. Kolthammer, A. Eckstein *et al.*, Quantum simulations with multiphoton fock states, *npj Quantum Inf.* **7**, 91 (2021).
- [33] A. Karnieli, Y. Li, and A. Arie, The geometric phase in nonlinear frequency conversion, *Front. Phys.* **17**, 12301 (2022).
- [34] H. Hübel, D. R. Hamel, A. Fedrizzi, S. Ramelow, K. J. Resch, and T. Jennewein, Direct generation of photon triplets using cascaded photon-pair sources, *Nature (London)* **466**, 601 (2010).
- [35] W. T. M. Irvine, K. Hennessy, and D. Bouwmeester, Strong Coupling between Single Photons in Semiconductor Microcavities, *Phys. Rev. Lett.* **96**, 057405 (2006).
- [36] O. Slattery, L. Ma, K. Zong, and X. Tang, Background and review of cavity-enhanced spontaneous parametric down-conversion, *J. Res. Natl. Inst. Stan.* **124**, 124019 (2019).
- [37] M. O. Scully and M. S. Zubairy, *Quantum Optics* (Cambridge University Press, Cambridge, England, 1997), pp. 111–115.
- [38] J. Eberly, Schmidt analysis of pure-state entanglement, *Laser Phys.* **16**, 921 (2006).
- [39] A. Christ, K. Laiho, A. Eckstein, K. N. Cassemiro, and C. Silberhorn, Probing multimode squeezing with correlation functions, *New J. Phys.* **13**, 033027 (2011).
- [40] P. P. Rohde, A. Schreiber, M. Štefaňák, I. Jex, and C. Silberhorn, Multi-walker discrete time quantum walks on arbitrary graphs, their properties and their photonic implementation, *New J. Phys.* **13**, 013001 (2011).
- [41] N. Quesada and J. E. Sipe, Effects of time ordering in quantum nonlinear optics, *Phys. Rev. A* **90**, 063840 (2014).
- [42] N. Quesada and J. E. Sipe, Time-Ordering Effects in the Generation of Entangled Photons Using Nonlinear Optical Processes, *Phys. Rev. Lett.* **114**, 093903 (2015).
- [43] D. A. Antonosyan, A. S. Solntsev, and A. A. Sukhorukov, Single-photon spontaneous parametric down-conversion in quadratic nonlinear waveguide arrays, *Opt. Commun.* **327**, 22 (2014).
- [44] Y. Wang and K. Fang, Few-photon transport via a multimode nonlinear cavity: Theory and applications, *Phys. Rev. A* **105**, 023713 (2022).
- [45] R. W. Boyd, *Nonlinear Optics* (Academic, New York, 2020), pp. 83–86.
- [46] T. Holstein and H. Primakoff, Field dependence of the intrinsic domain magnetization of a ferromagnet, *Phys. Rev.* **58**, 1098 (1940).
- [47] P. Jordan, Der Zusammenhang der symmetrischen und linearen gruppen und das mehrkörperproblem, *Z. Phys.* **94**, 531 (1935).
- [48] J. Schwinger and J. Schwinger, *Angular Momentum* (Springer, New York, 2001).
- [49] C. J. Turner, A. A. Michailidis, D. A. Abanin, M. Serbyn, and Z. Papić, Quantum scarred eigenstates in a rydberg atom chain: Entanglement, breakdown of thermalization, and stability to perturbations, *Phys. Rev. B* **98**, 155134 (2018).
- [50] W. Cai, J. Han, F. Mei, Y. Xu, Y. Ma, X. Li, H. Wang, Y. P. Song, Z.-Y. Xue, Z.-Q. Yin, S. Jia, and L. Sun, Observation of Topological Magnon Insulator States in a Superconducting Circuit, *Phys. Rev. Lett.* **123**, 080501 (2019).
- [51] L. J. Maczewsky, K. Wang, A. A. Dovgiiy, A. E. Miroshnichenko, A. Moroz, M. Ehrhardt, M. Heinrich, D. N. Christodoulides, A. Szameit, and A. A. Sukhorukov, Synthesizing multi-dimensional excitation dynamics and localization transition in one-dimensional lattices, *Nat. Photonics* **14**, 76 (2020).
- [52] M. S. Bahovadinov, D. V. Kurlov, S. I. Matveenko, B. L. Altshuler, and G. V. Shlyapnikov, Many-body localization transition in a frustrated xy chain, *Phys. Rev. B* **106**, 075107 (2022).

- [53] S. Zamani, R. Jafari, and A. Langari, Floquet dynamical quantum phase transition in the extended xy model: Nonadiabatic to adiabatic topological transition, *Phys. Rev. B* **102**, 144306 (2020).
- [54] W. P. Su, J. R. Schrieffer, and A. J. Heeger, Solitons in Polyacetylene, *Phys. Rev. Lett.* **42**, 1698 (1979).
- [55] A. Altland and M. R. Zirnbauer, Nonstandard symmetry classes in mesoscopic normal-superconducting hybrid structures, *Phys. Rev. B* **55**, 1142 (1997).
- [56] N. Bogoliubov, On the theory of superfluidity, *J. Phys.* **11**, 23 (1947).
- [57] A. Y. Kitaev, Unpaired majorana fermions in quantum wires, *Phys. Usp.* **44**, 131 (2001).
- [58] S. Bose, Quantum Communication through an Unmodulated Spin Chain, *Phys. Rev. Lett.* **91**, 207901 (2003).
- [59] M. Christandl, N. Datta, A. Ekert, and A. J. Landahl, Perfect State Transfer in Quantum Spin Networks, *Phys. Rev. Lett.* **92**, 187902 (2004).
- [60] A. Perez-Leija, R. Keil, A. Kay, H. Moya-Cessa, S. Nolte, L.-C. Kwek, B. M. Rodríguez-Lara, A. Szameit, and D. N. Christodoulides, Coherent quantum transport in photonic lattices, *Phys. Rev. A* **87**, 012309 (2013).
- [61] A. Kay, Perfect, efficient, state transfer and its application as a constructive tool, *Int. J. Quantum. Inform.* **08**, 641 (2010).
- [62] I. Pitsios, L. Banchi, A. S. Rab, M. Bentivegna, D. Caprara, A. Crespi, N. Spagnolo, S. Bose, P. Mataloni, R. Osellame *et al.*, Photonic simulation of entanglement growth and engineering after a spin chain quench, *Nat. Commun.* **8**, 1569 (2017).
- [63] C. Gogolin and J. Eisert, Equilibration, thermalisation, and the emergence of statistical mechanics in closed quantum systems, *Rep. Prog. Phys.* **79**, 056001 (2016).
- [64] A. J. Short and T. C. Farrelly, Quantum equilibration in finite time, *New J. Phys.* **14**, 013063 (2012).
- [65] C. K. Law, I. A. Walmsley, and J. H. Eberly, Continuous Frequency Entanglement: Effective Finite Hilbert Space and Entropy Control, *Phys. Rev. Lett.* **84**, 5304 (2000).
- [66] W. P. Grice, A. B. U'Ren, and I. A. Walmsley, Eliminating frequency and space-time correlations in multiphoton states, *Phys. Rev. A* **64**, 063815 (2001).
- [67] P. J. Mosley, J. S. Lundeen, B. J. Smith, P. Wasylczyk, A. B. U'Ren, C. Silberhorn, and I. A. Walmsley, Heralded Generation of Ultrafast Single Photons in Pure Quantum States, *Phys. Rev. Lett.* **100**, 133601 (2008).
- [68] B. T. Varcoe, S. Brattke, M. Weidinger, and H. Walther, Preparing pure photon number states of the radiation field, *Nature (London)* **403**, 743 (2000).
- [69] R. Uppu, L. Midolo, X. Zhou, J. Carolan, and P. Lodahl, Quantum-dot-based deterministic photon-emitter interfaces for scalable photonic quantum technology, *Nat. Nanotechnol.* **16**, 1308 (2021).
- [70] E. Waks, E. Diamanti, and Y. Yamamoto, Generation of photon number states, *New J. Phys.* **8**, 4 (2006).
- [71] X. Zhou, I. Dotsenko, B. Peaudecerf, T. Rybarczyk, C. Sayrin, S. Gleyzes, J. M. Raimond, M. Brune, and S. Haroche, Field Locked to a Fock State by Quantum Feedback with Single Photon Corrections, *Phys. Rev. Lett.* **108**, 243602 (2012).
- [72] M. Cosacchi, J. Wiercinski, T. Seidelmann, M. Cygorek, A. Vagov, D. E. Reiter, and V. M. Axt, On-demand generation of higher-order fock states in quantum-dot-cavity systems, *Phys. Rev. Res.* **2**, 033489 (2020).
- [73] G. Harder, T. J. Bartley, A. E. Lita, S. W. Nam, T. Gerrits, and C. Silberhorn, Single-Mode Parametric-Down-Conversion States with 50 Photons as a Source for Mesoscopic Quantum Optics, *Phys. Rev. Lett.* **116**, 143601 (2016).
- [74] J. Tiedau, T. J. Bartley, G. Harder, A. E. Lita, S. W. Nam, T. Gerrits, and C. Silberhorn, Scalability of parametric down-conversion for generating higher-order fock states, *Phys. Rev. A* **100**, 041802 (2019).
- [75] M. Uria, P. Solano, and C. Hermann-Avigliano, Deterministic Generation of Large Fock States, *Phys. Rev. Lett.* **125**, 093603 (2020).
- [76] B. Sain, C. Meier, and T. Zentgraf, Nonlinear optics in all-dielectric nanoantennas and metasurfaces: a review, *Adv. Photonics* **1**, 024002 (2019).
- [77] R. Yanagimoto, E. Ng, M. Jankowski, H. Mabuchi, and R. Hamerly, Temporal trapping: A route to strong coupling and deterministic optical quantum computation, *Optica* **9**, 1289 (2022).
- [78] G. Rempe, H. Walther, and N. Klein, Observation of Quantum Collapse and Revival in a One-Atom Maser, *Phys. Rev. Lett.* **58**, 353 (1987).
- [79] B. Jiang, S. Zhu, W. Wang, J. Li, C.-H. Dong, L. Shi, and X. Zhang, Room-temperature continuous-wave upconversion white microlaser using a rare-earth-doped microcavity, *ACS Photonics* **9**, 2956 (2022).
- [80] H.-Y. Liu, M. Shang, X. Liu, Y. Wei, M. Mi, L. Zhang, Y.-X. Gong, Z. Xie, and S. N. Zhu, Deterministic n-photon state generation using lithium niobate on insulator device, *Adv. Photonics Nexus* **2**, 016003 (2022).
- [81] C. Panuski, D. Englund, and R. Hamerly, Fundamental Thermal Noise Limits for Optical Microcavities, *Phys. Rev. X* **10**, 041046 (2020).
- [82] L. S. Madsen, F. Laudenbach, M. F. Askarani, F. Rortais, T. Vincent, J. F. Bulmer, F. M. Miatto, L. Neuhaus, L. G. Helt, M. J. Collins *et al.*, Quantum computational advantage with a programmable photonic processor, *Nature (London)* **606**, 75 (2022).
- [83] M. Eaton, A. Hossameldin, R. J. Birrittella, P. M. Alsing, C. C. Gerry, H. Dong, C. Cuevas, and O. Pfister, Resolution of 100 photons and quantum generation of unbiased random numbers, *Nat. Photonics* **17**, 106 (2023).
- [84] R. Cheng, Y. Zhou, S. Wang, M. Shen, T. Taher, and H. X. Tang, A 100-pixel photon-number-resolving detector unveiling photon statistics, *Nat. Photonics* **17**, 112 (2023).
- [85] J. Hloušek, M. Dudka, I. Straka, and M. Ježek, Accurate Detection of Arbitrary Photon Statistics, *Phys. Rev. Lett.* **123**, 153604 (2019).